

Thorium isotopes as tracers of particles dynamics and deep water circulation in the Indian sector of the Southern Ocean (ANTARES IV)

L. Coppola^{1,2*}, M. Roy-Barman^{1,3}, S. Mulsow⁴, P. Povinec⁵, C. Jeandel¹

¹ *LEGOS (CNRS/CNES/IRD/UPS), 14 av. E. Belin 31400 Toulouse, France*

² *LIG, Swedish Museum of Natural History, Box 50007, 10405 Stockholm, Sweden*

³ *LSCE/IPSL, Avenue de la Terrasse, 91198 Gif sur Yvette, France*

⁴ *Instituto de Geociencias, Universidad Austral de Chile, Valdivia, Chile*

⁵ *IAEA-Marine Environment Laboratory, 4 quai Antoine Ier, MC 98000, Monaco*

Submitted to Marine Chemistry (Final version August 2005)

Key words: Thorium-234; Thorium-230; marine particles; Southern Indian Ocean

*Corresponding author:

Phone: +46 8 5195 4234

Fax: +46 8 5195 4031

E-mail: laurent.coppola@nrm.se

Abstract

Dissolved and particulate samples were collected to study the distribution of thorium isotopes (^{234}Th , ^{232}Th and ^{230}Th) in the water column of the Indian sector of the Southern Ocean (from 42 to 47°S and from 60 to 66°E, north of the Polar Front) during Austral summer 1999. Vertical profiles of excess ^{230}Th ($^{230}\text{Th}_{\text{xs}}$) increases linearly with depth in surface water (0-100m) and a model was applied to estimate a residence time relative to the thorium scavenging (τ_{scav}). Low τ_{scav} in the Polar Front Zone (PFZ) are found, compared to those estimated in the Subtropical Front Zone (STZ). Changes in particle composition between the PFZ and STZ could influence the $^{230}\text{Th}_{\text{xs}}$ scavenging efficiency and explain this difference. An innovative coupling between ^{234}Th and $^{230}\text{Th}_{\text{xs}}$ was then used to simultaneously constrain the settling velocities of small (0.6-60 μm) and large (above 60 μm) particles. Although the different hydrological and biogeochemical regimes visited during the ANTARES IV cruise did not explain the spatial variation of sinking velocity estimates, our results indicate that less particles may reach the seafloor north ($60 \pm 2 \text{ m d}^{-1}$, station 8) than south of the Agulhas Return Current ($119 \pm 23 \text{ m d}^{-1}$ and $130 \pm 5 \text{ m d}^{-1}$ at stations 3 and 7, respectively). This information is essential for understanding particle transport and by extension, carbon export. In the deep water column, the $^{230}\text{Th}_{\text{xs}}$ concentrations did not increase linearly with depth, probably due to lateral transport of North Atlantic Deep Water (NADW) from the Atlantic to the Indian sector, which renews the deep waters and decreases the $^{230}\text{Th}_{\text{xs}}$ concentrations. A specific $^{230}\text{Th}_{\text{xs}}$ transport model is applied in the deep water column and allows us to assess a “travel time” of NADW ranging from 2 to 15 yrs.

1. Introduction

Rates of transport and interaction processes in the ocean can be evaluated with the radioactive decay of the natural Uranium-Thorium radioactive decay series (U-Th). Isotopes of soluble U (^{238}U and ^{234}U) decay to isotopes of highly particle-reactive Th (^{234}Th and ^{230}Th , respectively). In seawater, ^{234}Th and ^{230}Th are removed from the water column by adsorption onto settling particles (scavenging). The resulting U/Th disequilibria can be used to constrain the transport rates of particles and reaction processes between the solution and particulate phases (e.g. Cochran and Masqué, 2003). The short half-life of ^{234}Th (24 days) allows it to be used to estimate the vertical particle flux from the surface waters and the export of particulate organic carbon (POC) (Buesseler et al., 1992; Coale and Bruland, 1985; Moran et al., 1997a). The half-life of ^{230}Th (75,400 years) is much greater than its residence time in the ocean with respect to removal from the water column (10-50 yr; Anderson et al., 1983). Consequently, ^{230}Th can be used to evaluate thorium scavenging on settling particles and the renewal rates of water masses in the ocean (Anderson et al., 1983; Moran et al., 1997b; Rutgers van der Loeff and Berger, 1993; Scholten et al., 1995). A third isotope ^{232}Th (half-life 1.4×10^{10} years) is derived from the earth's crust and used to quantify the concentration of ^{230}Th contained within lithogenic particles (Chen et al., 1986).

The Southern Ocean is the largest oceanic high-nitrate low-chlorophyll (HNLC) region in the world and is known to contribute to the regulation of the atmospheric CO_2 via the biological pump (Metzl et al., 1999; Sigman and Boyle, 2000). The main objective of the French Southern Ocean Joint Global Ocean Flux Study (SO-JGOFS) carried out during the ANTARES IV (ANTArctic RESearch) cruise was to quantify the stock and the export of biogenic particles (C, N, Si) in relation to the biological pump of atmospheric CO_2 in the Indian sector of the Southern Ocean. In this sector, located from 40°E to 100°E and from 40°S to 60°S , the circumpolar path of the Antarctic Circumpolar Current (ACC) consists of three narrow jets associated with sharp fronts due to the presence of the Crozet and Kerguelen Islands (Park et al., 2002). The sampling area was located in

the north of the Crozet basin, which is one of the most dynamic areas of the Southern Ocean (Park and Gamberoni, 1995). This zone of strong physical gradients was chosen to study biogeochemical processes in a mesoscale circulation pattern (Park et al., 1993; Park et al., 2002).

In this paper, we report ^{232}Th and ^{230}Th data from seawater and particulate samples collected in surface and deep waters. ^{234}Th concentrations were already used to estimate the POC export (Coppola et al., 2005). Part of these ^{234}Th data are used in the present work and coupled with ^{230}Th to evaluate the settling velocity of marine particles in surface waters. In the deep water column, ^{230}Th concentrations allow an estimation of deep water renewal rates.

2. Sampling and analytical methods

2.1 Sampling sites

During the ANTARES IV cruise, both dissolved and particulate samples were collected in the Indian sector of the Southern Ocean. The sampling zone was located in the northwest of the Kerguelen Island bounded by 42-47°S and 60-66°E (Fig. 1), characterized from north to south by the confluence of the Agulhas Return Current (AF), the Subtropical Front (STF) and the Subantarctic Front (SAF), as described by Park et al. (1993, 1995, 1997, 2002). In the study area, these fronts converged into a narrow band from 100 to 200 km wide (Park et al., 2002). They delimited three zones characterized by different biological communities and distinct temperatures and salinities. The SAF has been located between the Polar Front (PF) and the STF, constituting the northern boundary of the Polar Front Zone (PFZ), that corresponds to the subduction of the Antarctic Intermediate Water (AAIW) from south to north. In the north of the SAF, the region was characterized by a strong temperature and salinity gradient. The Subantarctic Zone (SAZ) is delimited by the SAF and the STF. The Subtropical Zone (STZ) representing the warm oligotrophic waters has been positioned in the northern part of the STF. The AF forming a part of the STZ (Park et al., 1993; Park and Gamberoni, 1995) has been located north of two sampling stations. During the

ANTARES IV cruise (Fig. 1), three main stations (3, 7 and 8) were located respectively in the PFZ, in the STZ south of AF and in the STZ north of AF (Coppola et al., 2005). All biogeochemical characteristics of each zone/station were reported by Blain et al. (2002), Sedwick et al. (2002) and Leblanc et al. (2002). In this study, we present and discuss results on dissolved and particulate fractions of ^{234}Th , ^{230}Th and ^{232}Th measured on seawater and particles collected at three stations (3/4, 7/5 and 8/4).

2.2 Sampling and pre-concentration

The pre-concentration and analytical procedures were designed to allow the measurement of ^{230}Th , ^{232}Th as well as ^{234}Th on the same dissolved and particulate samples. The detailed procedure concerning ^{234}Th has already been published (Coppola et al., 2005). Seawater samples were collected with Niskin bottles and immediately filtered through acid-washed $0.6\mu\text{m}$ Nuclepore® polycarbonate membrane filters (diameter 143mm) using a Millipore® filtration system. Around 20-30L of seawater was used to analyze the small particulate fraction ($> 0.6\mu\text{m}$). All filtered seawater samples were acidified to pH 2 with 18 ml distilled HCl 6N per 10 L of sample to avoid thorium absorption on bottle walls. A ^{229}Th yield tracer and Fe carrier were added to the filtered seawater and allowed to equilibrate overnight. The pH was then raised to 8 with NH_3 solution (25%) to scavenge dissolved Th on $\text{Fe}(\text{OH})_3$ particles (Roy-Barman et al., 1996). After 24h of mixing, the precipitate was filtrated through another $0.6\mu\text{m}$ Nuclepore® filter that was used to measure the dissolved fraction of ^{234}Th (Coppola et al., 2005). For all samples, the iron precipitation was done 1-2 days after sample collection. Large particles ($>60\mu\text{m}$) were collected with *in situ* pumps (MARK II, Challenger Oceanic) at each station at depths ranging from 30 to 2400 m. Large volume seawater samples (500-2000L) were filtered through 143 mm diameter, $60\mu\text{m}$ mesh Teflon filters. Large particulates were subsequently washed off the filters ($0.6\mu\text{m}$ Nuclepore®) with pH 8 Milli-Q water. All filters containing particles and precipitate were dried and prepared for non-destructive beta counting (Rutgers van der Loeff and Moore, 1999; Coppola et al., 2005).

2.3 ^{230}Th and ^{232}Th analysis

After beta counting the samples for ^{234}Th (Coppola et al., 2005), ^{230}Th and ^{232}Th were analyzed on dissolved ($<0.6\mu\text{m}$) and particulate phases ($>0.6\mu\text{m}$ and $>60\mu\text{m}$). Particulate samples were dissolved with distilled 3N HCl. This solution was dried and the residue was dissolved in $\text{HNO}_3\text{-HCl}$. Residual solids (silica) were dissolved in HF-HNO_3 , dried after addition of HClO_4 and re-dissolved with distilled 7N HNO_3 . After complete dissolution, a ^{229}Th spike was added. For the dissolved fraction, the $\text{Fe}(\text{OH})_3$ precipitate was dissolved in distilled 6N HCl and the solution was divided into several fractions: 70% of the solution was used for the $^{230}\text{Th}\text{-}^{232}\text{Th}$ analysis, while the remaining fraction was used to determine the yield recovery and the contribution of ^{238}U in-growth for the ^{234}Th procedure (Coppola et al., 2005). For dissolved and particulate samples, Th was purified with an anionic ion exchange column (Roy-Barman et al., 1996). The concentrations of ^{232}Th and ^{230}Th contained in all fractions were measured by Thermal Ionization Mass Spectrometry (Roy-Barman et al., 2002). Typical blanks were $^{232}\text{Th} = 52 \pm 3 \text{ pg L}^{-1}$ (blank correction = 0-9 %) and $^{230}\text{Th} = 1.3 \pm 0.5 \text{ fg L}^{-1}$ (blank correction = 0-40 %).

3. Results

^{230}Th and ^{232}Th concentrations in dissolved and particulate samples are shown in Table 1. Thorium concentrations are expressed in pg L^{-1} for ^{232}Th ($1 \text{ pg L}^{-1} = 0.000246 \text{ dpm m}^{-3}$) and in fg L^{-1} for ^{230}Th ($1 \text{ fg L}^{-1} = 0.0459 \text{ dpm m}^{-3}$). $^{230}\text{Th}/^{232}\text{Th}$ isotopic ratios are expressed in mol/mol. In order to determine ^{230}Th concentrations derived solely from *in situ* decay of ^{238}U , we corrected measured ^{230}Th concentrations for contributions by lithogenic material, excess ^{230}Th ($^{230}\text{Th}_{\text{xs}}$), using the following equation:

$$^{230}\text{Th}_{\text{xs}} = ^{230}\text{Th}_{\text{measured}} - ^{232}\text{Th}_{\text{measured}} \times \left(\frac{^{230}\text{Th}}{^{232}\text{Th}} \right)_{\text{litho}} \quad (1)$$

with $(^{230}\text{Th}/^{232}\text{Th})_{\text{litho}} = 4.4 \times 10^{-6}$ based on a mean $^{232}\text{Th}/^{238}\text{U} = 3.8$ atom/atom of the continental crust (Andersson et al., 1995).

The dissolved ^{232}Th concentrations ranged from 25 to 70 pg L^{-1} . The particulate ^{232}Th concentrations were lower than the dissolved ^{232}Th in all sampling stations and the highest values were measured in the STZ.

At all stations, the dissolved $^{230}\text{Th}_{\text{xs}}$ concentrations increase linearly with depth until 200m and range from 0 to 5 fg L^{-1} . These values are similar to those observed between 0 and 500 m in the Atlantic sector (north of 50°S) of the Southern Ocean (Rutgers van der Loeff and Berger, 1993). On the other hand, the dissolved $^{230}\text{Th}_{\text{xs}}$ concentrations profiles in the deep layer do not increase linearly with depth. Below 1500 m, the dissolved $^{230}\text{Th}_{\text{xs}}$ profiles has a concave shape, typical of ^{230}Th profiles from the Atlantic and Pacific sectors of the Southern Ocean (Chase et al., 2003a; Rutgers van der Loeff and Berger, 1993). These deep layer profile shapes contrast with those observed in many other oceanic regions, where $^{230}\text{Th}_{\text{xs}}$ concentrations increase linearly with depth (Cochran et al., 1987; Mangini and Key, 1983; Nozaki et al., 1981; Roy-Barman et al., 1996). In the bottom layer, the dissolved $^{230}\text{Th}_{\text{xs}}$ concentrations are higher in the PFZ than in the STZ (15 fg L^{-1} and 9-12 fg L^{-1} , respectively). The $^{230}\text{Th}_{\text{xs}}$ concentrations in small particles represented, on average, less than 10 % of the dissolved $^{230}\text{Th}_{\text{xs}}$ concentrations at all stations except in the surface waters of the STZ where they were comparable to the dissolved $^{230}\text{Th}_{\text{xs}}$ concentrations. In the large particle fractions, the ^{232}Th and $^{230}\text{Th}_{\text{xs}}$ concentrations are very low and represented less than 1% of the ^{232}Th and $^{230}\text{Th}_{\text{xs}}$ contained in the small particles.

In the following section, we will consider the total particles (small and large) to be roughly equivalent to the small particles since the ^{234}Th and $^{230}\text{Th}_{\text{xs}}$ concentrations measured on small particles ($>0.6\mu\text{m}$) are ~100 times higher than those on large ones ($> 60\mu\text{m}$) and large particle data is not available from all depths at all stations for each isotope (see Table 1).

4. Discussion

4.1 The $^{230}\text{Th}_{\text{xs}}$ - ^{234}Th coupling in surface waters

$^{230}\text{Th}_{\text{xs}}$ and ^{234}Th in seawaters are produced *in situ* from ^{234}U and ^{238}U , respectively, with a constant and well-defined production rate. Their oceanic chemical behaviours are a priori comparable, although their half-lives differ by about five orders of magnitude (75,400 yrs and 24 d, respectively). Their water column distributions can be further examined using a reversible model in which the dissolved and particulate fractions of $^{230}\text{Th}_{\text{xs}}$ and ^{234}Th are exchanged by adsorption and desorption (Bacon and Anderson, 1982; Coale and Bruland, 1985; Nozaki et al., 1981; Nozaki et al., 1987). It should be noted that the values of parameters involved in this model can vary if $^{230}\text{Th}_{\text{xs}}$ and ^{234}Th concentrations are used separately. This is illustrated by the following example. In the two-box model describing the dissolved and particulate Th phases, the settling velocities of particles deduced separately from ^{234}Th and $^{230}\text{Th}_{\text{xs}}$ are given by the following equations (Bacon and Anderson, 1982; Coale and Bruland, 1985; Nozaki et al., 1981):

$$V_{234} = \frac{J_{234} \times h}{^{234}\text{Th}} \quad (2)$$

$$V_{230} = \frac{J_{230} \times h}{^{230}\text{Th}_{\text{xs}}} \quad (3)$$

where J_{234} and J_{230} are the removal fluxes of ^{234}Th and $^{230}\text{Th}_{\text{xs}}$ ($J=P-\lambda\text{Th}$ with P the production rate and λ the decay rate of Th; note that with λ_{230} being very low, J_{230} is similar to P_{230}), $^{230}\text{Th}_{\text{xs}}$ and ^{234}Th are the concentrations of the nuclides in the total particulate phase (equivalent to the small particles) and depth, h , in the water column. In these equations, we assume steady state and no physical transport (especially no lateral transport of ^{230}Th and ^{234}Th). We first used the total ^{234}Th concentrations measured at stations 3, 7 and 8 in surface water (0-100m) by Coppola et al. (2005) and Eq. (2) in order to estimate total particle settling velocities, which ranged from 2.6 to 5.2 m d^{-1} . The settling velocities for the same pool of particles deduced from the total $^{230}\text{Th}_{\text{xs}}$ concentrations

and Eq. (3) range from 0.2 to 2.5 m d⁻¹. We further calculated the settling velocities for large particles from a three-box model (e.g. Nozaki et al, 1987), the three boxes being dissolved, small and large particles. In the three-box model, we assume that the settling velocity of small particles is negligible, at steady state, and are not affected by physical transport terms. This model leads to Eq. (2) and (3) where $^{230}\text{Th}_{\text{xs}}$ and ^{234}Th are the concentrations of the nuclides in the large particulate fraction. Using the $^{230}\text{Th}_{\text{xs}}$ and ^{234}Th concentrations measured in the large particle pool in Eq. (2) and (3), resulted in settling velocities ranging from 40 to 97 m d⁻¹ and from 14 to 330 m d⁻¹ for ^{234}Th and $^{230}\text{Th}_{\text{xs}}$, respectively.

The calculations based on large and small particle pools yield very different results. The settling velocity calculated with ^{234}Th and $^{230}\text{Th}_{\text{xs}}$ for large particles are more widely varied than those for small particles. It may be due to the large uncertainties (poor vertical resolution and analytical uncertainties) associated with the large particle pool and/or to the short residence time of the large particles (making it more probable that the large particle flux is not exactly at steady state). A more extensive temporal and vertical sampling is necessary to clarify these conclusions. For the small particles, the differences between the independent settling velocity estimates from ^{234}Th and $^{230}\text{Th}_{\text{xs}}$ are less important than for large particles, suggesting that ^{234}Th is mainly controlled by production and decay and that the assumption to neglect the lateral transport of $^{230}\text{Th}_{\text{xs}}$ from 0 to 100 m is reasonable. The above estimates and comparisons between models and Th isotopes suggest that the coupling of ^{230}Th and ^{234}Th measured in distinct pools (dissolved, small and large fractions) may reduce the above disagreement and improve current calculations of settling velocities.

Therefore, the goal of this study is to include simultaneous measurements of both $^{230}\text{Th}_{\text{xs}}$ and ^{234}Th into two independent equations describing Th systematics within a three box model (where each box represents a distinct fraction of Th: dissolved, small and large particles) in the upper 100 m in order to better constrain the settling velocities of small and large particles.

4.1.1 The $^{230}\text{Th}_{\text{xs}}$ - ^{234}Th model description

In previous studies, on the use of multiple Th isotopes, such as ^{230}Th - ^{228}Th and ^{234}Th - ^{228}Th , were used to constrain adsorption/desorption rates, i.e. aggregation/disaggregation and the remineralization processes in different oceanic regions (Clegg et al., 1991; Cochran et al., 1993; Cochran et al., 2000; Luo et al., 1995; Murnane et al., 1996; Murnane et al., 1994; Trimble et al., 2004). Only a few studies have used a direct coupling between $^{230}\text{Th}_{\text{xs}}$ and ^{234}Th because the sampling and measurement techniques for these nuclides are quite different (Murnane et al., 1996; Trimble et al., 2004). In addition, those studies used a fixed settling velocity term in order to constrain the adsorption/desorption rates (Clegg and Whitfield, 1990).

In the present study, the combination of $^{230}\text{Th}_{\text{xs}}$ - ^{234}Th was applied from 0 to 100m only, as the half-life of ^{234}Th is too short to make this tracer usable in deep waters (Fig. 2). In addition, the distribution of $^{230}\text{Th}_{\text{xs}}$ in the deep ocean of the ANTARES IV region is influenced by lateral advection (as we shall discuss later). In the following calculations, we will neglect the horizontal advection and diffusion terms and focus only on vertical transport of settling particles. This hypothesis is supported by the linear increase of $^{230}\text{Th}_{\text{xs}}$ with depth in the shallow water..

To describe the $^{230}\text{Th}_{\text{xs}}$ - ^{234}Th coupling in surface waters (0-100 m), we used a simple reversible particle exchange model where the main difference between the $^{230}\text{Th}_{\text{xs}}$ and ^{234}Th equations is the negligibility of ^{230}Th decay rate relative to other terms in the ^{230}Th equation. At steady state, the equations are (Fig. 3):

$$\frac{d^{234}\text{Th}_t}{dt} = P_{234} - \lambda_{234}^{234}\text{Th}_t - v \frac{\partial^{234}\text{Th}_s}{\partial z} - V \frac{\partial^{234}\text{Th}_l}{\partial z} = 0 \quad (4)$$

$$\frac{d^{230}\text{Th}_t}{dt} = P_{230} - v \frac{\partial^{230}\text{Th}_s}{\partial z} - V \frac{\partial^{230}\text{Th}_l}{\partial z} = 0 \quad (5)$$

where Th_s , Th_l and Th_t are the concentrations of ^{234}Th and $^{230}\text{Th}_{\text{xs}}$ integrated from 0 to 100 m in small (0.6-60 μm), large (>60 μm) and total fractions, respectively. P_{234} and P_{230} are the ^{234}Th and $^{230}\text{Th}_{\text{xs}}$ production rates from ^{238}U (25.2 dpm $\text{L}^{-1} \text{y}^{-1}$) and ^{234}U (0.56 fg $\text{L}^{-1} \text{y}^{-1}$) and λ_{234} represents

the radioactive decay of ^{234}Th (0.028 d^{-1} and negligible for $^{230}\text{Th}_{\text{xs}}$). These equations were combined to simultaneously solve v and V , which correspond to the settling velocities of small and large particles.

4.1.2 The settling velocities for small and large particles

^{234}Th and $^{230}\text{Th}_{\text{xs}}$ concentrations were applied to Eq. (4) and (5) by dividing the water column into depth intervals based on the sampling depths (0-100m) at stations 3, 7 and 8. The uncertainties were propagated using a Monte Carlo simulation method. The resulting settling velocities, taken at 100m for all stations, ranged from -0.5 to 1.6 m d^{-1} and from 60 to 130 m d^{-1} for small and large particles, respectively (Table 2). As expected, lower settling velocities were obtained for the small particles relative to the large ones. At station 8, we estimated a negative value for the small particles. As already suggested above, this could be due to the low resolution of the $^{230}\text{Th}_{\text{xs}}$ and ^{234}Th vertical profiles for large particles in surface water or from the upwelling of water, which will affect the vertical transport of small particles with low settling velocity. You (1999) showed that north of 45°S , dianeutral upwelling is predominant in the thermocline water, but only occurs at $1.3 \times 10^{-3} \text{ m d}^{-1}$. This is low compared to the settling velocity estimated for small particles at station 8 (-0.5 m d^{-1}). Consequently, we hypothesize that it is the low resolution of $^{230}\text{Th}_{\text{xs}}$ and ^{234}Th measurements in surface waters and the assumption of steady state in the model that results in the negative settling velocity calculated at station 8. This may indicate that the uncertainty of $\pm 0.20 \text{ m d}^{-1}$ for this value is underestimated. If the uncertainty of sinking velocity at stations 7 and 3 have also been underestimated, it would leave open the possibility that all sinking velocity of small particles are not significantly different from zero. However, more data are required to test this hypothesis.

The results also show significant spatial variability for settling velocities of both small and large particles among stations 3, 7 and 8. In fact, large particle settling velocities estimated at stations 3 and 7 are two times higher than those estimated at station 8 (Table 2).

Such variations are not clearly explained by the different biogeochemical conditions observed during the ANTARES IV cruise. In summer, the frontal zone of the Indian sector was characterized by distinct regimes of macronutrients (nitrate and phosphate) and iron exerting a primary and/or secondary limitation on phytoplankton (mainly diatoms) growth and accumulation (Sedwick et al., 2002). In addition, Leblanc et al. (2002) observed a low diatom contribution to the primary productivity and hence sinking particle flux in the PFZ and within the SAF/STF. Direct microscopic observations, indicate that the community was dominated by microplanktonic flagellates (dinoflagellates, ciliates, etc.) at stations 7 and 8 and nanoflagellates at station 3 during the summer. High POC/Chl *a* ratios further suggests the presence of degraded organic matter and/or a predominance of heterotrophs at all stations. This phytoplankton distribution is not consistent with the observed differences in settling velocities.

Zooplankton distributions also do not explain the variations in settling velocity between the stations (3 and 7 versus 8). Labat et al. (2002) observed in ANTARES IV that copepods dominated and had a maximum of biomass in the PFZ (station 3). At this site, *Calanus* was the main population while *Pleuromma borealis* and *P. abdominalis* characterized those north of the STF (stations 7 and 8). Thus similar populations of zooplankton are unlikely to cause the observed differences in large particle settling velocity.

Panagiotopoulos et al. (2002) observed that the OC mineralization of large particles by bacteria was more rapid at station 7 than at station 3. In the STZ waters, sea surface temperatures appeared high enough to allow a fast recycling of BSi and an efficient microbial loop in the surface waters was observed (Panagiotopoulos et al., 2002; Sempéré et al., 2000). If correct, than OC mineralization in surface waters is not a major factor in the control of the settling velocity of large particles.

Consequently it may not be possible to explain the spatial difference in sinking velocity between the different hydrological and biogeochemical regimes visited during the Antares IV cruise. Nonetheless, our results indicate that, because of the sinking velocity, less particles reach the seafloor north of the Agulhas Return Current. This information plays a critical role in the context of particle transport and by extension, OC export, in these regimes.

4.1.3 $^{230}\text{Th}_{\text{xs}}$ and ^{234}Th affinity for large particles and POC export

From the calculated settling velocities of large particles, it is possible to estimate the POC fluxes exported at 100m and to compare them with those derived from ^{234}Th - ^{238}U disequilibria (Coppola et al., 2005). From station 3 to 8, the resulting POC fluxes range from 1.39 to 0.32 $\text{mmolC m}^{-2} \text{d}^{-1}$, while the ^{234}Th -derived POC fluxes range from 1.77 to 0.94 $\text{mmolC m}^{-2} \text{d}^{-1}$. Both ranges of values are comparable. This confirms the hypotheses that i) the large settling particles are more appropriate to estimate POC export and that ii) the $\text{POC}/^{234}\text{Th}$ ratio of the large particles is appropriate for use in the ^{234}Th disequilibrium approach. The same calculation shows that the calculated POC flux from small settling velocity particles is 2-15 times lower than the ^{234}Th -derived POC flux estimated with $\text{POC}/^{234}\text{Th}$ on small particles.

Using the estimated settling velocities and the $\text{POC}/^{234}\text{Th}$ ratios estimated by Coppola et al. (2005) on small and large particles, it is possible to estimate the proportions of $^{230}\text{Th}_{\text{xs}}$, ^{234}Th and POC on small and large particles. The calculations are based on the ratio between the $^{230}\text{Th}_{\text{xs}}$ and ^{234}Th concentrations in the small and large particles. The proportion of POC in both particle fractions is estimated from the multiplication of $\text{POC}/^{234}\text{Th}$ ratio and the ^{234}Th concentrations in the respective particle fractions. The results suggest that for all three stations, a larger fraction of ^{234}Th (2-9%) than $^{230}\text{Th}_{\text{xs}}$ (0.3-1.7%) is on the large particles. This point is surprising since particle-water partitioning is expected to be the same for both ^{234}Th and ^{230}Th (Guo et al., 1995). One possibility could be that in the recent past (timescale of ^{234}Th decay), the creation of new large particles

dominated the particle dynamics in surface waters where total ^{234}Th concentrations are higher than $^{230}\text{Th}_{\text{xs}}$. However, this idea is not consistent with the observed similarity of POC and $^{230}\text{Th}_{\text{xs}}$ distributions. Nevertheless, such $^{230}\text{Th}_{\text{xs}}$ distributions vs. POC concentrations should be observed over a longer period of time, since it has been previously shown that ^{234}Th partitions between solution, colloidal and particle phases in a manner broadly similar to that of organic carbon (Guo et al., 1997; Roy-Barman, submitted). Consequently, although the ^{230}Th concentration is important for calculation of the settling velocity, our Th repartition vs. particle size confirms that ^{234}Th is the most appropriate for estimation of POC export using the POC/ ^{234}Th ratio on large sinking particles.

4.2 Renewal rate in the deep water column

Tracers such as CFC (chlorofluorocarbon) and dissolved oxygen are often used to estimate the circulation and ventilation of water masses (Boswell and Smythe-Wright, 2002; Rintoul et al., 2001; Tanhua et al., 2004). In some studies, $^{230}\text{Th}_{\text{xs}}$ concentrations have been used as a particle and water mass tracer to study the water circulation in the Southern Ocean (Chase et al., 2003a; Chase et al., 2003b; Honjo et al., 2000; Rutgers van der Loeff et al., 1997). Here, we use $^{230}\text{Th}_{\text{xs}}$ concentrations in the deep ocean in order to understand advection and scavenging processes in the Southern Indian Ocean where the frontal zone induces variable productivity regimes and hence, particle fluxes to sediments.

In the deep waters of stations 3, 7 and 8, the total $^{230}\text{Th}_{\text{xs}}$ concentrations does not increase linearly with depth: total ^{230}Th concentrations are lower than those expected using the simple $^{230}\text{Th}_{\text{xs}}$ scavenging model, suggesting that lateral transport is occurring. These type of $^{230}\text{Th}_{\text{xs}}$ profiles are typically observed in or close to deep waters formation areas (Moran et al., 1997b; Rutgers van der Loeff and Berger, 1993; Scholten et al., 1995; Volger et al., 1998). The main deep waters observed in the Indian sector of the Southern Ocean are the North Atlantic Deep Water (NADW) and the Circumpolar Deep Water (CDW) (Fig. 4). Profiles of potential temperature versus salinity in

ANTARES IV indicate that NADW, characterized by a maximum of salinity, was observed in the deep water column at stations 3, 7 and 8 (Fig. 5a). In term of mass transport, the NADW exported from the South Atlantic represents 20% of the total southward flow of deep water into the Southern Ocean. At 60°E, the remaining fraction of NADW (10%) is found at 40°S, corresponding to the ANTARES IV sampling area. At the same location, You (2000) observed that a large fraction of NADW is transformed to CDW (Circumpolar Deep Water) suggesting that this area is a source of CDW. This mass transformation creates a renewal mechanism of NADW, visible in the ^{230}Th data.

The $^{230}\text{Th}_{\text{xs}}$ production term, $P_{^{230}\text{Th}}$, is constant in seawater ($0.56 \text{ fg L}^{-1} \text{ y}^{-1}$). Hence, the total $^{230}\text{Th}_{\text{xs}}$ profiles in the deep water column depend only on scavenging and lateral/vertical transport of $^{230}\text{Th}_{\text{xs}}$. The renewal rate (τ_w) is defined as the travel time of the water mass that has been laterally transported between the Atlantic sector (the major source of Southern Ocean deep water) to the Indian sector, where samples were collected. This renewal rate is different from the ventilation rate, which corresponds to the time since the water mass has been in contact with the atmosphere. A model describing the transport of $^{230}\text{Th}_{\text{xs}}$ in the deep water can be used to estimate a renewal time of NADW.

The $^{230}\text{Th}_{\text{xs}}$ contained in deep water in the sampling area can be distinguished using a plot of $^{230}\text{Th}_{\text{xs}}$ against the density parameter σ_{2000} (Fig. 5b). It indicates that the deep water column was renewed from 1500m depth (z_0) by a lateral transport of NADW ($\sigma_{2000} = 37.0$) from west to east, which injects total $^{230}\text{Th}_{\text{xs}}$ (noted $^{230}\text{Th}_i$). To estimate a renewal rate of the deep water column, we apply the model derived from Rutgers van der Loeff et al. (1993):

$$\frac{d^{230}\text{Th}_t}{dt} = P_{^{230}\text{Th}} - \frac{h}{2\tau_s} \times \frac{d^{230}\text{Th}_t}{dz} + \frac{(^{230}\text{Th}_i - ^{230}\text{Th}_t)}{\tau_w} \quad (6)$$

where $^{230}\text{Th}_t$ is the total (dissolved and particle) fraction of $^{230}\text{Th}_{\text{xs}}$, h the water column depth (m) and τ_s the residence time of ^{230}Th (years) with respect to scavenging. In this equation, the ^{230}Th decay rate (λ_{230}) is negligible compared to other terms and was not included in Eq (6). In this case, $\tau_s = h/2VK$, where K represents the $^{230}\text{Th}_p/^{230}\text{Th}_t$ ratio constant with depth (0.13), and $^{230}\text{Th}_p$

and $^{230}\text{Th}_t$ are the particulate and total (dissolved + small particles) fraction of $^{230}\text{Th}_{\text{xs}}$. V is the settling velocity of sinking particles. In the Southern Ocean, we assume simply that the source water of NADW is located in the South Atlantic, in the northern part of the Polar Front (Rutgers van der Loeff and Berger, 1993). During the German JGOFS expedition ANT VIII/3, the NADW was found at a depth, z_i , of around 2500 m at station 1751 and 1755 (on the same isopycnal $\sigma_{2000} = 37.0$). They measured a total $^{230}\text{Th}_{\text{xs}}$ concentration of 14-16 fg L^{-1} , which will we use as the initial concentration of total ^{230}Th , $^{230}\text{Th}_i$ (Rutgers van der Loeff and Berger, 1993). Assuming steady state, the distribution of $^{230}\text{Th}_{\text{xs}}$ with depth (z) is:

$$^{230}\text{Th}_t(z) = (^{230}\text{Th}_i + P_{^{230}\text{Th}} \tau_w) \times \left[1 - \exp\left(-\frac{2\tau_s(z-z_0)}{\tau_w h}\right) \right] + ^{230}\text{Th}_t(z_0) \times \exp\left(-\frac{2\tau_s(z-z_0)}{\tau_w h}\right) \quad (7)$$

Figure 6 compares the total $^{230}\text{Th}_{\text{xs}}$ profile expected from Eq. (7) with the experimental values at stations 3, 7 and 8 and τ_s and τ_w have been adjusted to obtain the best fit between the modelled and measured $^{230}\text{Th}_{\text{xs}}$ profiles. The results depend on station location. In the PFZ (station 3), $\tau_s = 20$ -60 yrs and $\tau_w = 4$ -10 yrs. In the STZ at stations 7 and 8, τ_s and τ_w are similar (7-8 years and 2-15 years, respectively). The upper limit of the renewal time (15 yrs) estimated in ANTARES IV is consistent with the NADW current speed (1 cm s^{-1}) calculated from the South Atlantic to the Indian sectors by the dynamic model of Park and Guernier (2001). The scavenging residence time calculated in the PFZ indicates that the ^{230}Th scavenging process is longer than the deep water renewal rate and corresponds to a particle settling velocity of $0.7 - 1.8 \text{ m d}^{-1}$ for the entire water column. This result is in agreement with the settling velocity of small particles estimated from the $^{230}\text{Th}_{\text{xs}}$ - ^{234}Th model in surface waters (see section 4.1.2). The scavenging residence time found in the PFZ is consistent to the $^{230}\text{Th}_{\text{xs}}$ distribution in the deep sea (20-40 yrs; Bacon and Anderson, 1982). It is also similar to that Rutgers van der Loeff et al. (1993) observed in the Atlantic sector of the Southern Ocean. This suggests that the $^{230}\text{Th}_{\text{xs}}$ concentrations of deep water in the PFZ are predominantly controlled by renewal processes rather than by the scavenging of particles. In contrast, in the STZ, τ_s is shorter and corresponds to particle settling velocity of 5.3 m d^{-1} . This

suggests that in this area, scavenging is more efficient and influences the $^{230}\text{Th}_{\text{xs}}$ concentrations of the deep water.

5. Conclusion

The Indian sector of the Southern Ocean shows that particle transport in the surface water varies regionally, in correlation with the position of the fronts. Our estimations of settling velocities of small and large particles provided by using both ^{234}Th - $^{230}\text{Th}_{\text{xs}}$ indicated that fewer particles may reach the seafloor north of the Agulhas Return Current, an essential component for the study of particle transport and sedimentation. Our results do not appear to be explained by the biogeochemical regimes existing in the ANTARES IV area. The ^{230}Th - ^{234}Th model was limited by the low vertical resolution of $^{230}\text{Th}_{\text{xs}}$ and ^{234}Th concentrations in surface waters. Consequently, for future studies, a more precise description is recommended to interpret the ^{234}Th - $^{230}\text{Th}_{\text{xs}}$ data as tracers of particle dynamics. Distribution of ^{230}Th contains quantitative information not only on the particle behaviour in the ocean but also on deep circulation and renewal. In this study, a transport model of $^{230}\text{Th}_{\text{xs}}$ was applied in the deep water column to explain the concave $^{230}\text{Th}_{\text{xs}}$ vertical profiles. The model confirms that a significant part of $^{230}\text{Th}_{\text{xs}}$ is transported laterally by the NADW. The travel time of NADW from the Atlantic sector to the Indian sector was estimated as a rapid and not negligible process, consistent with previous studies. In future Southern Ocean projects, more ^{230}Th data in the deep layer should be evaluated and compared with previous studies located in others sectors of the Southern Ocean in order to constrain the global deep water circulation around the Antarctica.

Acknowledgment

We are grateful to K. Leblanc, C. Panagiotopoulos and R. Sempéré for sharing their ANTARES IV biogeochemical data. We thank Pierre Brunet for his assistance with the mass spectrometer and M. Souhaut for his support in the clean laboratory. Thanks to Y. Park, R. Francois and M. Rutgers van der Loeff for providing helpful comments on the lateral transport of the deep water mass. We also wish to thank Drs. Tom Trull and Nicolas Savoye for their insightful and careful comments on the manuscript. The IAEA is grateful for the support provided to its Marine Environment Laboratory by the Government of the Principality of Monaco.

References

- Anderson, R.F., Bacon, M.P. and Brewer, P.G., 1983. ^{230}Th and ^{231}Pa from the open ocean. *Earth and Planetary Science Letters*, 62: 7-23.
- Andersson, P.S., Wasserburg, G.J., Chen, J.H., Papanastassiou, D.A. and Ingri, J., 1995. ^{238}U - ^{234}U and ^{232}Th - ^{230}Th in the Baltic sea and in river water. *Earth and Planetary Science Letters*, 130: 217-234.
- Bacon, M.P. and Anderson, R.F., 1982. Distribution of thorium isotopes between dissolved and particulate forms in the deep sea. *J. Geophys. Res.*, 87: 2045-2056.
- Boswell, S.M. and Smythe-Wright, D., 2002. The tracer signature of Antarctic Bottom Water and its spread in the Southwest Indian Ocean: Part I—CFC-derived translation rate and topographic control around the Southwest Indian Ridge and the Conrad Rise. *Deep Sea Research Part I*, 49(3): 555-573.
- Buesseler, K.O., Bacon, M., Cochran, J.K. and Livingston, H.D., 1992. Carbon and nitrogen export during the JGOFS North Atlantic Bloom Experiment estimated from ^{234}Th - ^{238}U disequilibria. *Deep Sea Research*, 39: 1115-1137.
- Chase, Z., Anderson, R.F., Fleisher, M.Q. and Kubik, P.W., 2003a. Scavenging of ^{230}Th , ^{231}Pa and ^{10}Be in the Southern Ocean (SW Pacific sector): The importance of particle flux, particle composition and advection. *Deep-Sea Research II*, 50(3-4): 739-768.
- Chase, Z., Anderson, R.F., Fleisher, M.Q. and Kubik, P.W., 2003b. Accumulation of biogenic and lithogenic material in the Pacific sector of the Southern Ocean during the past 40,000 years. *Deep-Sea Research II*, 50(3-4): 799-832.
- Chen, J.H., Edwards, R.L. and Wasserburg, G.J., 1986. ^{238}U - ^{234}U and ^{232}Th in seawater. *Earth and Planetary Science Letters*, 80: 241-251.
- Clegg, S.L. and Whitfield, M., 1990. A generalized model for the scavenging of trace metals in the open ocean-I. particle cycling. *Deep Sea Research*, 37: 809-832.
- Clegg, S.L., Bacon, M. and Whitfield, M., 1991. Application of a generalized scavenging model to thorium isotope and particle data at equatorial and high-latitude sites. *J. Geophys. Res.*, 96(C11): 20655-20670.
- Coale, K.H. and Bruland, K.W., 1985. ^{234}Th - ^{238}U disequilibria within the California current. *Limnology and Oceanography*, 30: 22-33.
- Cochran, J.K., Livingston, H.D., Hirschberg, D.J. and Surprenant, L.D., 1987. Natural and anthropogenic radionuclide distributions in the northwest Atlantic Ocean. *Earth Planet. Sci. Lett.*, 84: 135-152.
- Cochran, J.K., Buesseler, K.O., Bacon, M.P. and Livingston, H.D., 1993. Thorium isotopes as indicators of particle dynamics in the upper ocean: results from the JGOFS North Atlantic Bloom Experiment. *Deep-Sea Res.*, 40: 1569-1595.
- Cochran, J.K. et al., 2000. Short-lived thorium isotopes (^{234}Th , ^{228}Th) as indicators of POC export and particle cycling in the Ross Sea, Southern Ocean. *Deep-Sea Research II*, 47(15-16): 3451-3490.

- Cochran, J.K. and Masqué, P., 2003. Short-lived U/Th series radionuclides in the Ocean: tracers for scavenging rates, export fluxes and particle dynamics. In: B. Bourdon, G.M. Henderson, C.C. Lundstrom and S.P. Turner (Editors), Uranium series geochemistry. Reviews in Mineralogy and Geochemistry, USA, pp. 461-530.
- Coppola, L., Roy-Barman, M., Mulsow, S., Povinec, P. and Jeandel, C., 2005. Low particulate organic carbon export in the frontal zone of the Southern Ocean (Indian Sector) revealed by ^{234}Th . Deep Sea Research I, 52: 51-68.
- Dezileau, L. and Reyss, J.L., 2003. The $^{231}\text{Pa}_{\text{ex}}/^{230}\text{Th}_{\text{ex}}$ ratio as a proxy for past changes in opal fluxes. Marine Chemistry, 81: 105-117.
- Ganachaud, A. and Wunsch, C., 2000. Improved estimates of global ocean circulation, heat transport and mixing from hydrographic data. Nature, 408, 453-456.
- Guo, L., Santschi, P.H., Baskaran, M. and Zindler, A., 1995. Distribution of dissolved and particulate ^{230}Th and ^{232}Th in seawater from the Gulf of Mexico and off Cape Hatteras as measured by SIMS. Earth and Planetary Science Letters, 133: 117-128.
- Guo, L.D., Santschi, P.H. and Baskaran, M., 1997. Interactions of thorium isotopes with colloidal organic matter in oceanic environments. Colloids and Surfaces a-Physicochemical and Engineering Aspects, 120(1-3): 255-271.
- Honjo, S., Francois, R., Manganini, S., Dymond, J. and Collier, R., 2000. Particle fluxes to the interior of the Southern Ocean in the Western Pacific sector along 170W. Deep-Sea Research II, 47: 3521-3548.
- Labat, J.P. et al., 2002. Mesoscale distribution of zooplankton in the Sub-Antarctic Frontal system in the Indian part of the Southern Ocean: a comparison between optical plankton counter and net sampling. Deep Sea Research I, 49: 735-749.
- Leblanc, K. et al., 2002. Particulate biogenic silica and carbon production rates and particulate matter distribution in the Indian sector of the Subantarctic Ocean. Deep Sea Research II, 49(16): 3189-3206.
- Luo, S., Ku, T.-L., Kusakabe, M., Bishop, J. and Yang, Y.-L., 1995. Tracing particle cycling in the upper ocean with ^{230}Th and ^{228}Th : an investigation in the equatorial Pacific along 140°W. Deep Sea Research II, 42(2-3): 805-829.
- Mangini, A. and Key, R.M., 1983. ^{230}Th profile in the Atlantic Ocean. Earth and Planetary Science Letters, 62(3): 377-384
- Mayzaud, P. et al., 2002. Carbon intake by zooplankton. Importance and role of zooplankton grazing in the Indian sector of the Southern Ocean. Deep Sea Research II, 49: 3169-3187
- Metzl, N., Tilbrook, B. and Poisson, A., 1999. The annual fCO_2 cycle and the air-sea CO_2 flux in the sub-Antarctic Ocean. Tellus Series B Chemical and physical meteorology, 51(4): 849-861.
- Moran, S.B., Charette, M.A., Hoff, J.A., Edwards, R.L. and Landing, W.M., 1997a. Distribution of ^{230}Th in the Labrador Sea and its relation to ventilation. Earth and Planetary Science Letters, 150: 151-160.

- Moran, S.B., Ellis, K.M. and Smith, J.N., 1997b. $^{234}\text{Th}/^{238}\text{U}$ disequilibrium in the Central Arctic Ocean: implications for particulate organic carbon export. *Deep Sea Research II*, 44(8): 1593-1606.
- Murname, R.J., Cochran, J.K., Buesseler, K.O. and Bacon, M.P., 1996. Least-squares estimates of thorium, particles and nutrient cycling rate constants from the JGOFS North Atlantic Bloom Experiment. *Deep Sea Research I*, 43(2): 239-258.
- Nozaki, Y., Horibe, Y. and Tsubota, H., 1981. The water column distribution of thorium isotopes in the western North Pacific. *Earth Planet. Sci. Lett.*, 54: 203-216.
- Nozaki, Y., Yang, H.-S. and Yamada, M., 1987. Scavenging of thorium in the ocean. *J. Geophys. Res.*, 92: 772-778.
- Panagiotopoulos, C. et al., 2002. Bacterial degradation of large particles in the Southern Indian Ocean using in vitro incubations experiments. *Organic Geochemistry*, 33(8): 985-1000.
- Park, Y., Gamberoni, L. and Charriaud, E., 1993. Frontal Structure, Water Masses and Circulation in the Crozet Basin. *J. Geophys. Res.*, 98(C7): 12,361-12,385.
- Park, Y.H. and Gamberoni, L., 1995. Large-scale circulation and its variability in the south Indian Ocean from TOPEX/POSEIDON altimetry. *Journal of Geophysical Research*, 100(12): 24911-24929.
- Park, Y.H. and Gamberoni, L., 1997. Cross-frontal exchange of Antarctic Intermediate Water and Antarctic Bottom Water in the Crozet Basin. *Deep-Sea Research II*, 44: 963-986.
- Park, H.-Y. and Guernier, J.M., 2001. A simple method for diagnosing the bottom current field of the world's oceans. *Journal of Physical Oceanography*, 31(4): 972-991.
- Park, Y.H., Lebourcier, V., Pollard, R., Read, J. and Fèvre, J.L., 2002. A quasi-synoptic view of the frontal circulation in the Crozet Basin during the ANTARES-4 cruise. *Deep Sea Research II*, 49(9-10): 1823-1842.
- Rintoul, S.R. and Bullister, J.L., 1999. A late winter hydrographic section from Tasmania to Antarctica. *Deep Sea Research I*, 46: 1417-1454.
- Rintoul, S.R., Hughes, C.W. and Olbers, D., 2001. The Antarctic circumpolar current system. In: G. Siedler, J. Church and J. Gould (Editors), *Ocean, circulation and climate observing and modelling the Global Ocean*. Academic Press, pp. 271-302.
- Roy-Barman, M., Chen, J.H. and Wasserburg, G.J., 1996. ^{230}Th - ^{232}Th systematics in the Central Pacific Ocean: the sources and the fates of thorium. *Earth and Planetary Science Letters*, 139: 351-363.
- Roy-Barman, M., Coppola, L. and Souhaut, M., 2002. Thorium isotopes in the Western Mediterranean Sea: an insight in the marine particle dynamics. *Earth and Planetary Science Letters*, 196: 161-174.
- Roy-Barman, M., Jeandel, C., Souhaut, M., Rutgers van der Loeff, M.M., Voege, I., Leblond, N. and Freyrier, R., submitted. Vertical evolution of Thorium isotope scavenging in the NE Atlantic ocean (POMME experiment). *Earth and Planetary Science Letters*.
- Rutgers van der Loeff, M.M. and Berger, G., W., 1993. ^{230}Th and ^{231}Pa near the Antarctic Polar Front in the South Atlantic. *Deep Sea Res.*, 40: 339-357.

- Rutgers van der Loeff, M.M., Freidrich, J. and Bathmann, U.V., 1997. Carbon export during the spring bloom at the Antarctic polar front, determined with the natural tracer ^{234}Th . *Deep Sea Res.*, 44: 457-478.
- Scholten, J., Rutgers van der Loeff, M.M. and Michel, A., 1995. Distribution of ^{230}Th and ^{231}Pa in the water column in relation to the ventilation of the deep Arctic basins. *Deep Sea Research Part II*, 42(6): 1519-1531
- Sedwick, P. N. et al., 2002. Resource limitation of phytoplankton growth in the Crozet Basin, Subantarctic Southern Ocean. *Deep Sea Research II*, 49(16): 3327-3349
- Sempéré, R., Yoro, S.C., Wambeke, F.V. and Charrière, B., 2000. Microbial decomposition of large organic particles in the northwestern Mediterranean Sea: an experimental approach. *Marine Ecology and Progress Series*, 198: 61-72.
- Sigman, D. and Boyle, E., 2000. Glacial/Interglacial variations in atmospheric carbon dioxide. *Nature*, 407: 859-869.
- Tanhua, T., Olsson, K.A. and Fogelqvist, E., 2004. A first study of SF₆ as a transient tracer in the Southern Ocean. *Deep Sea Research Part II*, 51(22-24): 2683-2699.
- Trimble, S.M., Baskaran, M. and Porcelli, D., 2004. Scavenging of thorium isotopes in the Canada Basin of the Arctic Ocean. *Earth Planet. Sci. Lett.*, 222: 915-932.
- Volger, S., Scholten, J., Rutgers van der Loeff, M. and Mangini, A., 1998. ^{230}Th in eastern North Atlantic: the importance of water ventilation in the balance of ^{230}Th . *Earth Planet. Sci Lett.*, 156: 61-47.
- You, Y., 1999. Dianeutral mixing, transformation and transport of the deep water of the Indian Ocean. *Deep Sea Research Part I*, 46: 109-148.
- You, Y., 2000. Implications of the deep circulation and ventilation of the Indian Ocean on the renewal mechanism of North Atlantic Deep Water. *Journal of Geophysical Research*, 105(C10): 23895-23926.

FIGURE CAPTIONS

Figure 1. Location of stations in the sampling area. The arrows represent the position of front observed during the campaign ANTARES IV (SAF: Subantarctic Front, STF: Subtropical Front, AF: Agulhas Return Current).

Figure 2. Vertical profiles of $^{230}\text{Th}_{\text{xs}}$ (fg/l) and ^{234}Th (dpm/l) concentrations in dissolved, small and large particles (noted with respective subscribes d, s and l). The uncertainty is expressed at 2 standard deviations (Table 1)

Figure 3. Box model of the $^{230}\text{Th}_{\text{xs}}$ and ^{234}Th concentrations in dissolved, small and large particulate pools. The radioactive decay is represented by λ . k_1 , k_{-1} , β_2 and β_{-2} are the first-order rate constants to thorium adsorption, desorption and to particle aggregation and disaggregation, respectively. v and V are the sinking velocities of small and large particles, respectively.

Figure 4. (a) Schematic deep water circulation of NADW/CDW and AABW in the Indian sector (from Park and Gamberoni, 1995). The sampling area ANTARES IV is symbolized by the hatched square. (b) Circulation model illustrating the inflow rates of NADW from the South Atlantic to the Indian sector (from Ganachaud and Wunsch, 2000) with the total $^{230}\text{Th}_{\text{xs}}$ concentrations.

Figure 5. Theta-salinity profiles (a) and density diagram (σ_{2000}) versus total $^{230}\text{Th}_{\text{xs}}$ concentrations (b) at stations 3, 7 and 8. The North Atlantic Deep Water (NADW) is characterized by a salinity maximum.

Figure 6. Model prediction of the vertical total $^{230}\text{Th}_{\text{xs}}$ (dissolved + small particle) profiles in the deep water column at stations 3, 7 and 8. The fit of the model with the total $^{230}\text{Th}_{\text{xs}}$ concentrations allows to estimate the residence time of $^{230}\text{Th}_{\text{xs}}$ relative to the scavenging (τ_s) and to the renewal of the deep water column (τ_w). The solid lines represent the lower and upper limits of the model predictions.

Table 1. ^{232}Th (pg l^{-1}), $^{230}\text{Th}_{\text{xs}}$ (fg l^{-1}) and $^{230}\text{Th}/^{232}\text{Th}$ ratios (mol mol^{-1}) in dissolved, small and large particles (noted d, s and l). Each station is characterised by the number of operation/cast (#OPA), the geographical position and the seafloor depth. The station 7 corresponds to the composite of 2 casts of a single visit.

Depth (m)	$^{232}\text{Th}_d \pm 2\sigma$ (pg l^{-1})	$^{232}\text{Th}_s \pm 2\sigma$ (pg l^{-1})	$^{232}\text{Th}_l \pm 2\sigma$ ($\text{pg } 10^{-2}\text{l}^{-1}$)	$^{230}\text{Th}_{\text{ssd}} \pm 2\sigma$ (fg l^{-1})	$^{230}\text{Th}_{\text{sss}} \pm 2\sigma$ (fg l^{-1})	$^{230}\text{Th}_{\text{ssl}} \pm 2\sigma$ ($\text{fg } 10^{-2}\text{l}^{-1}$)	$(^{230}\text{Th}/^{232}\text{Th})_d$ $\times 10^4 \pm 2\sigma$	$(^{230}\text{Th}/^{232}\text{Th})_s$ $\times 10^4 \pm 2\sigma$	$(^{230}\text{Th}/^{232}\text{Th})_l$ $\times 10^4 \pm 2\sigma$
St3 (#OPA077, 45.66°S, 63.11°E, 4320 m)									
10	63.4 ± 0.7	8.9 ± 0.1		0.22 ± 0.28	0.02 ± 0.03		0.10 ± 0.05	0.17 ± 0.27	
30	33.6 ± 0.7	16.3 ± 1.2		1.08 ± 0.30	0.01 ± 0.02		0.40 ± 0.10	0.18 ± 0.70	
50	43.7 ± 1.7	0.9 ± 0.1		1.66 ± 0.43	0.13 ± 0.21		0.45 ± 0.11		
100	34.7 ± 0.9	5.6 ± 0.1	0.66 ± 0.03	2.30 ± 2.58	0.05 ± 0.08	0.05 ± 0.05	0.74 ± 0.78	0.26 ± 0.27	0.96 ± 0.97
200	39.0 ± 3.1	7.3 ± 0.1		4.86 ± 0.64	0.10 ± 0.14		1.33 ± 0.20	0.38 ± 0.40	
500	68.9 ± 4.3	1.6 ± 0.1		4.94 ± 0.80	0.41 ± 0.18		0.81 ± 0.13	3.12 ± 1.40	
1000			0.81 ± 0.27			0.41 ± 0.14			
1500	54.8 ± 3.0	10.0 ± 0.3	34.3 ± 1.3	8.14 ± 1.45	1.20 ± 0.24	4.15 ± 1.93	1.58 ± 0.29	1.27 ± 0.25	1.33 ± 0.60
2500	33.7 ± 1.5	6.2 ± 0.1	25.1 ± 2.1	15.60 ± 1.47	2.04 ± 0.77	2.52 ± 1.05	4.75 ± 0.49	3.30 ± 1.20	1.11 ± 0.45
3500	48.5 ± 2.7	7.1 ± 0.1		15.05 ± 1.91	2.22 ± 0.33		3.20 ± 0.44	3.21 ± 0.48	
St7 (#OPA240/244, 44.01°S, 64.73°E, 4551/4798 m)									
10	33.2 ± 2.5	29.3 ± 0.7	2.01 ± 0.05	0.77 ± 0.27	0.63 ± 0.33	0.07 ± 0.10	0.31 ± 0.09	0.27 ± 0.12	0.52 ± 0.62
40	34.7 ± 4.7	13.7 ± 0.2		0.43 ± 0.54	0.63 ± 0.25		0.20 ± 0.18	0.52 ± 0.19	
100	38.9 ± 1.6	8.7 ± 0.1	0.78 ± 0.02	1.56 ± 0.48	0.32 ± 0.18	0.11 ± 0.05	0.47 ± 0.13	0.43 ± 0.21	1.65 ± 0.73
200	44.8 ± 1.7	5.3 ± 0.3	3.19 ± 0.08	2.73 ± 0.87	0.27 ± 0.17	0.07 ± 0.08	0.68 ± 0.20	0.60 ± 0.35	0.34 ± 0.31
500	37.2 ± 0.9	6.9 ± 0.1	2.96 ± 0.06	4.22 ± 0.65	0.36 ± 0.20	0.09 ± 0.07	1.22 ± 0.18	0.60 ± 0.31	0.59 ± 0.38
1500	37.3 ± 0.9	14.4 ± 0.1	26.8 ± 0.4	5.79 ± 0.50	1.64 ± 0.19	2.06 ± 0.12	1.64 ± 0.14	1.20 ± 0.14	0.83 ± 0.05
2500	36.8 ± 0.8	8.9 ± 0.1	30.9 ± 0.4	11.41 ± 1.24	1.52 ± 0.18	1.72 ± 0.24	3.21 ± 0.35	1.79 ± 0.20	0.66 ± 0.09
3500	49.6 ± 0.6	11.0 ± 0.2		11.97 ± 0.81	2.00 ± 0.32		2.50 ± 0.17	1.90 ± 0.30	
St8 (#OPA324, 42.91°S, 63.08°E, 4998 m)									
10	48.4 ± 2.7	31.1 ± 0.9		1.39 ± 0.35	0.90 ± 0.31		0.36 ± 0.08	0.34 ± 0.10	
46	28.6 ± 1.7			0.99 ± 0.48	1.50 ± 0.60		0.43 ± 0.19		
100	55.3 ± 4.0	25.0 ± 0.2	37.6 ± 0.4	4.54 ± 0.91	0.64 ± 0.19	1.07 ± 0.12	0.89 ± 0.18	0.31 ± 0.08	0.35 ± 0.03
200	46.2 ± 1.0	12.1 ± 0.2	62.1 ± 1.4	4.60 ± 0.91	0.13 ± 0.16	1.91 ± 0.44	1.07 ± 0.20	0.17 ± 0.15	0.36 ± 0.07
500	37.2 ± 0.5	8.2 ± 0.1	39.2 ± 0.5	6.34 ± 0.32	0.10 ± 0.18	0.86 ± 0.13	1.80 ± 0.09	0.19 ± 0.26	0.28 ± 0.04
1000			61.3 ± 1.1			0.83 ± 0.49			0.25 ± 0.11
1500	46.6 ± 1.0	34.9 ± 0.4	65.2 ± 1.0	4.38 ± 0.53	2.50 ± 0.90	4.09 ± 0.20	1.02 ± 0.12	0.74 ± 0.26	0.69 ± 0.03
2500	23.9 ± 1.9	14.9 ± 0.3	128.8 ± 2.6	10.55 ± 1.48	1.81 ± 0.88	11.72 ± 0.44		1.29 ± 0.60	0.98 ± 0.04
3500	66.4 ± 1.5	15.2 ± 0.2		9.15 ± 1.48	4.11 ± 0.53		1.45 ± 0.24	2.78 ± 0.35	

Table 2. The sinking velocities (m d^{-1}) v and V and the derived particulate organic carbon (POC) fluxes ($\text{mmolC m}^{-2} \text{d}^{-1}$) for the small and large particles at stations 3, 7 and 8 (noted respectively with subscript s and l). The standard deviations are due to the errors propagation of the $^{230}\text{Th}_{\text{xs}}$ and ^{234}Th data.

Station	Depth range (m)	v (m d^{-1})	V (m d^{-1})	$(\text{POC})_s$	$(\text{POC})_l$
3	0-100	1.6 ± 1.1	119 ± 23	$9.0 \pm 6.0 \times 10^{-3}$	1.39 ± 0.27
7	0-100	0.14 ± 0.04	130 ± 5	$1.1 \pm 0.3 \times 10^{-3}$	0.68 ± 0.03
8	0-100	-0.49 ± 0.20	60 ± 2	$-3.1 \pm 1.3 \times 10^{-3}$	0.32 ± 0.01

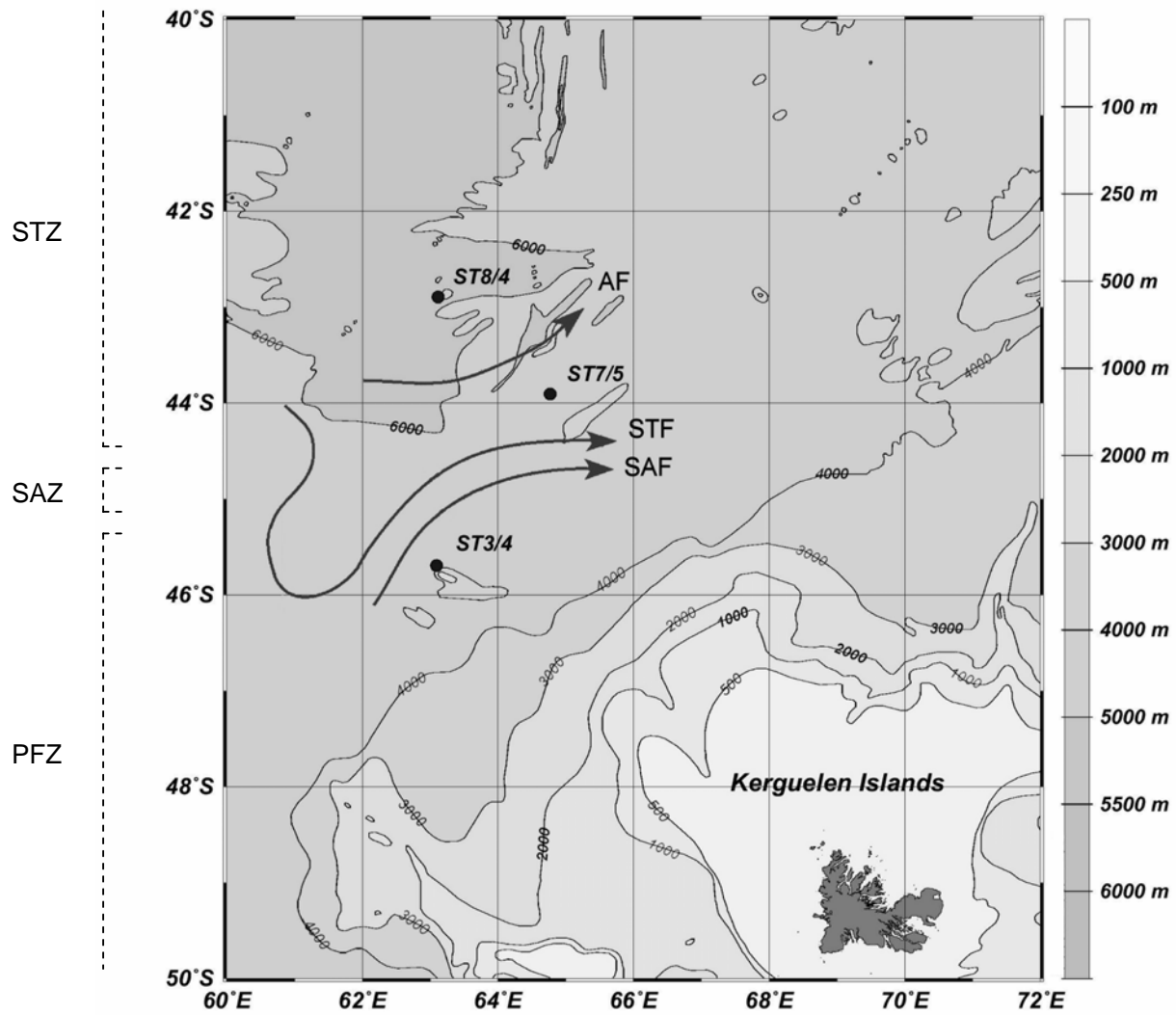


Fig. 1

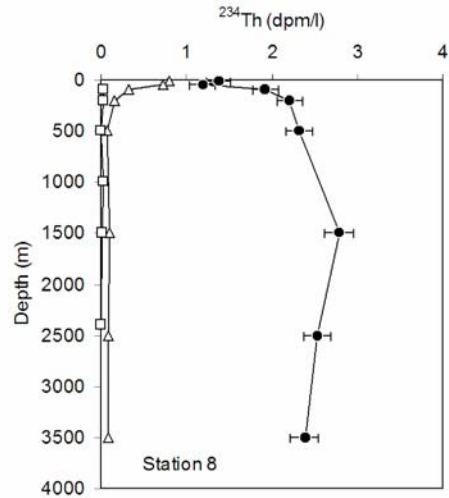
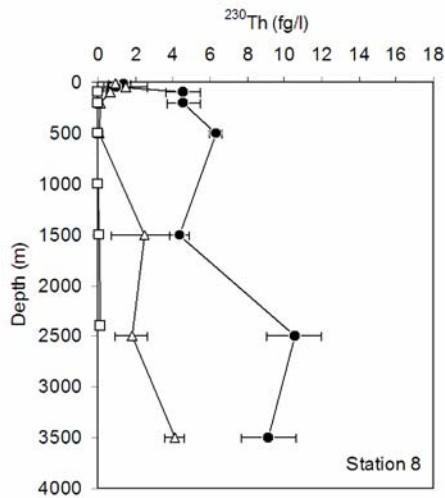
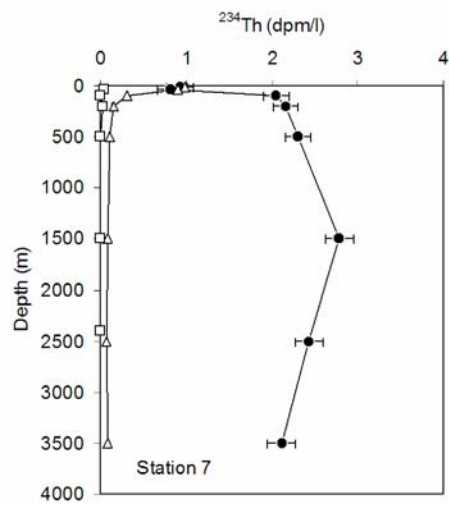
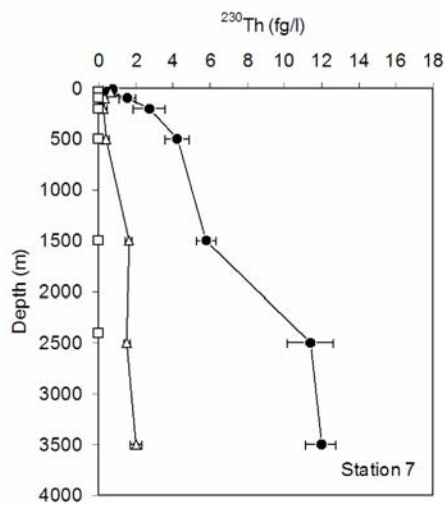
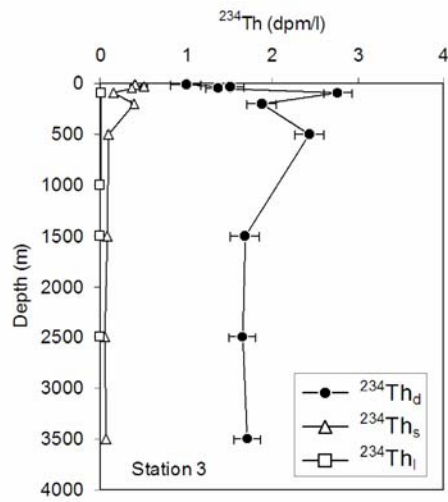
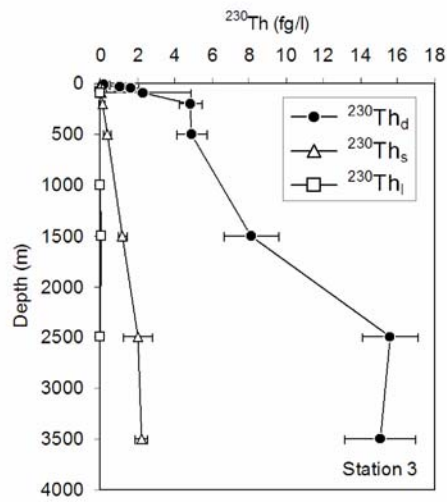


Fig. 2

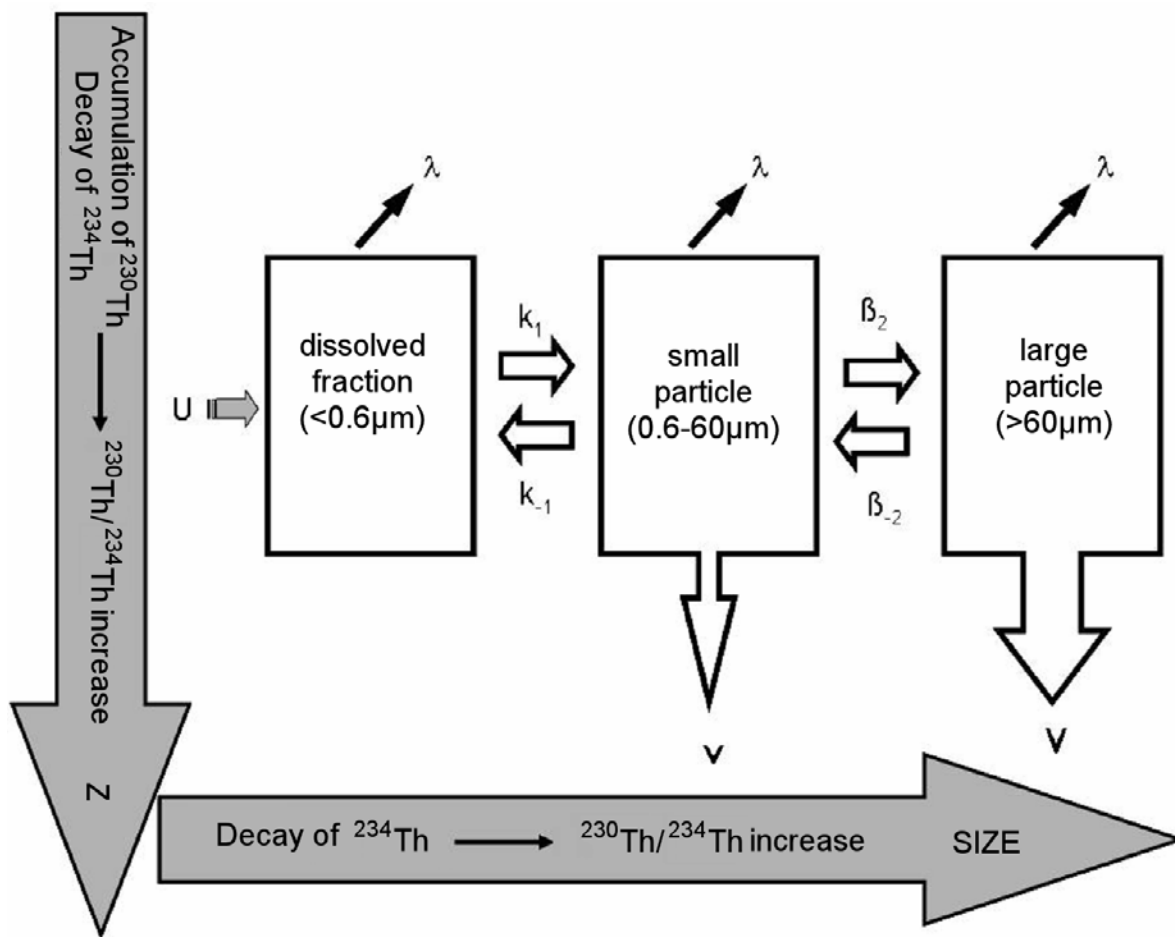


Fig. 3

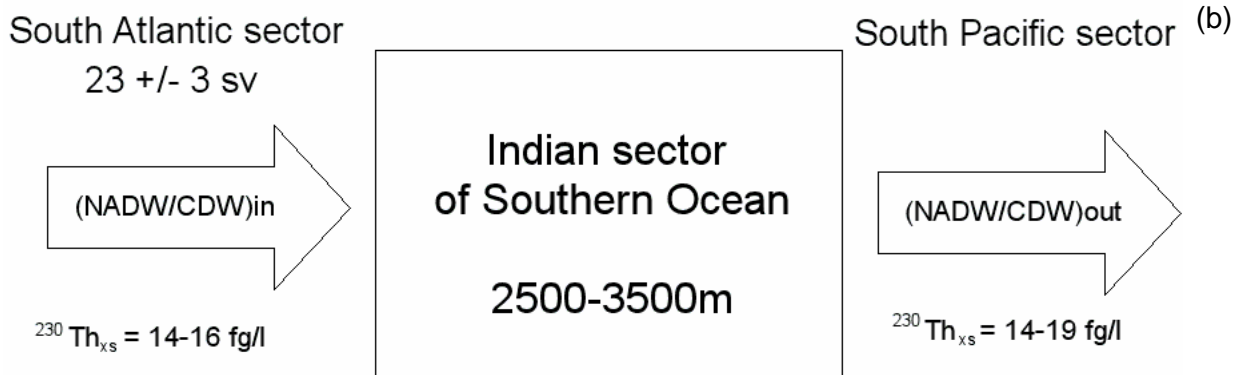
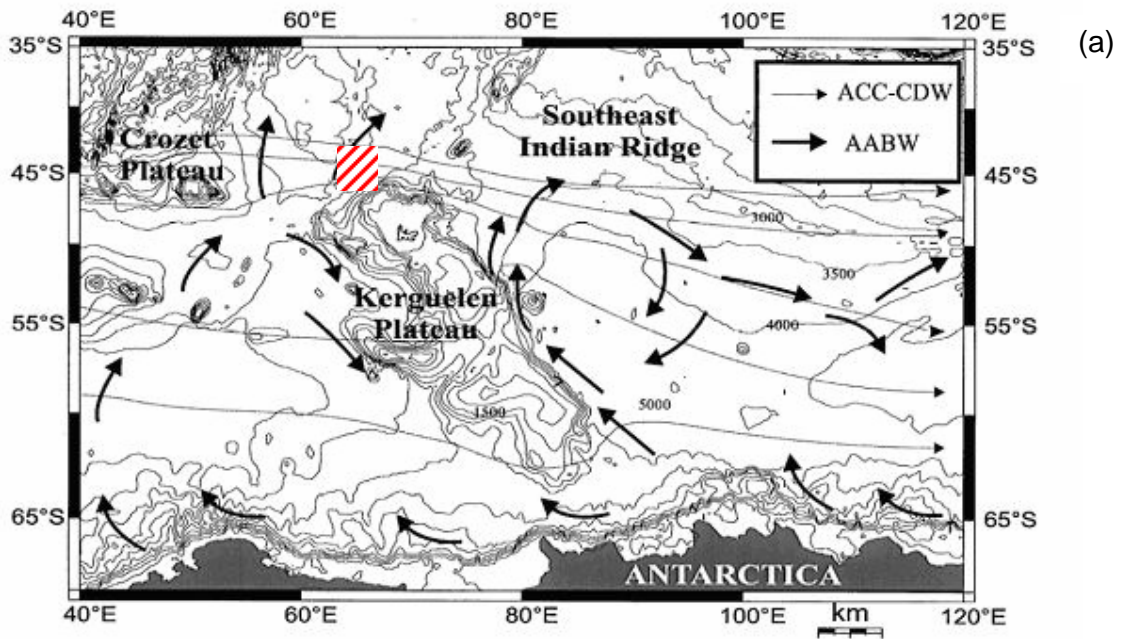
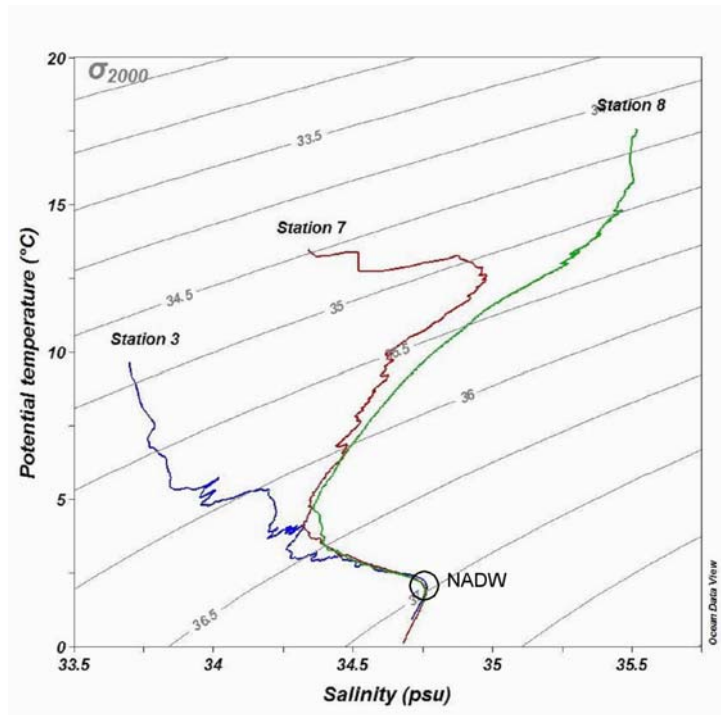
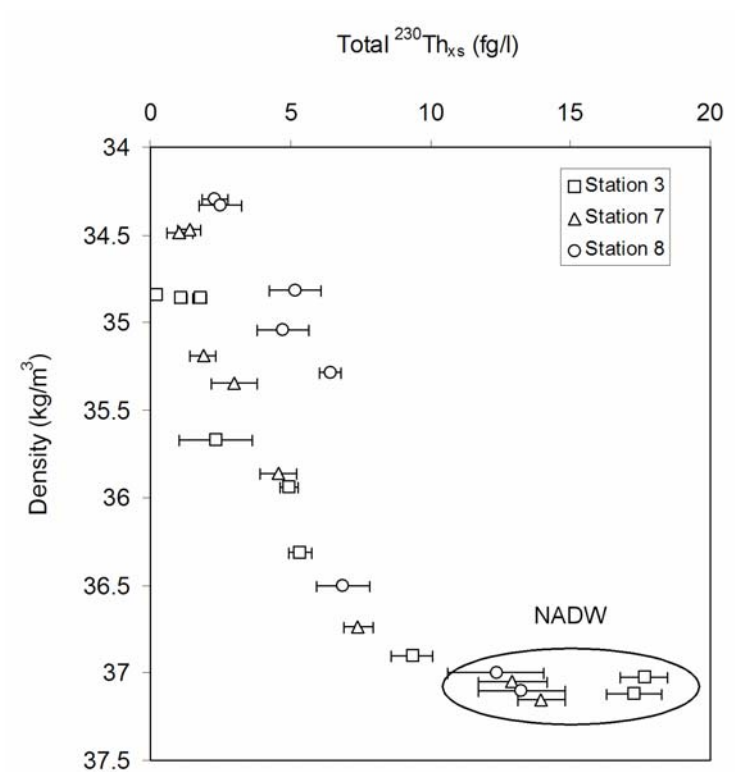


Fig. 4



(a)



(b)

Fig. 5

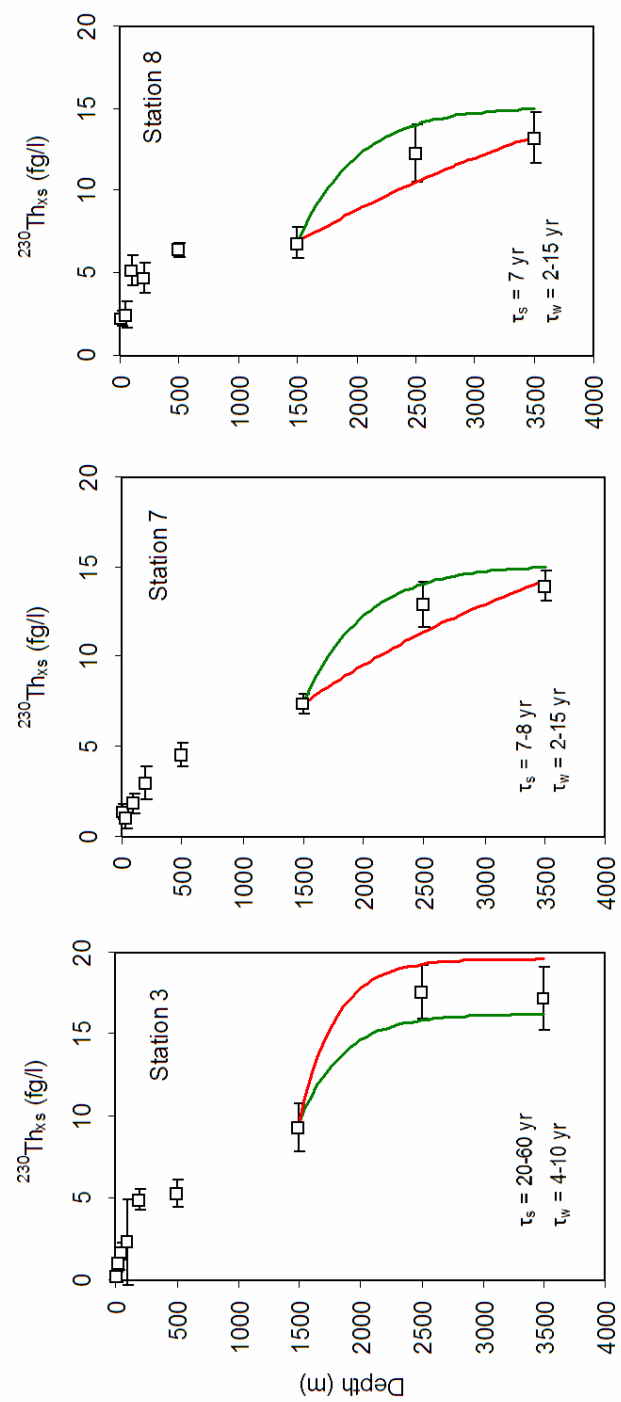


Fig. 6